Dynamic hysteresis from bistability in an antiferromagnetic spinor condensate

Tomasz Świsłocki,[1] Andrzej Zembrzuski,[1] Michał Matuszewski,[2] and Emilia Witkowska[2]
[1]*Faculty of Applied Informatics and Mathematics, Warsaw University of Life Sciences, Ulica Nowoursynowska 159, 02-786 Warsaw, Poland*
[2]*Institute of Physics, Polish Academy of Sciences, Aleja Lotnikow 32/46, 02-668 Warsaw, Poland*

(Received 22 December 2017; published 29 March 2018)

We study the emergence of hysteresis during the process of quantum phase transition from an antiferromagnetic to a phase-separated state in a spin-1 Bose-Einstein condensate of ultracold atoms. We explicitly demonstrate the appearance of a hysteresis loop with various quench times, showing that it is rate independent for large magnetizations only. In other cases, scaling of the hysteresis loop area is observed, which we explain by using the Kibble-Zurek theory in the limit of small magnetization. The effect of an external harmonic trapping potential is also discussed.

DOI: 10.1103/PhysRevA.97.033629

The classic example of hysteresis is the relation of the applied magnetic field to the magnetization in solid-state ferromagnetic materials. Hysteresis can also occur in different situations as a product of a fundamental physical mechanism, such as a phase transition, or a result of imperfections or degradations. Hysteresis occurs in two forms: rate-dependent and rate-independent hysteresis. In the rate-independent case, two or more metastable energy states are separated by an energy barrier. When an external driving force moves the system from one metastable state to another, the system exhibits the history-dependent behavior. The rate-independent hysteresis of supercurrent in a rotating, superfluid Bose-Einstein condensate was observed and has been proclaimed as a milestone in the advancement of atomtronic circuitry [1–3]. A recent experiment [4] has also demonstrated the rate-independent hysteresis when a Bose-Einstein condensate is placed in a double-well potential. On the other hand, the observation of rate-dependent hysteresis could provide insight into the out-of-equilibrium dynamics of the system.

Spinor condensates are composed of N atoms in several Zeeman components with a given hyperfine spin F and magnetic numbers m_F. The global ground state of the $F = 1$ system is classified as ferromagnetic or antiferromagnetic, depending on the sign of spin-dependent interactions. The magnetization longitudinal with respect to magnetic field M is approximately conserved in the system and acts as an independent external parameter. This conservation law comes from the spin rotational symmetry of contact interactions when dipole-dipole interactions are neglected. Consequently, in contrast to solid-state magnetic materials, classical hysteresis is impossible in spinor $F = 1$ condensates. However, a weak magnetic field drives the system to the transition from an antiferromagnetic ground state to a state where domains of atoms with different spin projections separate [5]. The phase transition is specific due to the region of bistability in which the antiferromagnetic and phase separated states are both metastable [6].

In this paper we investigate the emergence of hysteresis from bistability during the phase transition in an antiferromagnetic spin-1 condensate. The system is already recognized as useful for quantum technology tasks. By employing numerical simulations within the truncated Wigner approximation, we demonstrate the appearance of rate-independent hysteresis for large magnetizations only, when the bistability region is widest. In the limit of small magnetizations the bistability region disappears; however, competition between the characteristic timescale of driving and the relaxation time of the system leads to the emergence of rate-dependent hysteresis. We show that in this case, the hysteresis loop area is subject to a universal scaling law. We estimate the scaling of the hysteresis loop area based on the Kibble-Zurek (KZ) theory [7–9], similarly to [10]. The situation changes when the system is enclosed in an external trapping potential, as it eliminates the separation of the two metastable energy states and the rate-independent hysteresis loop becomes impossible to observe. The scaling of the rate-dependent hysteresis area in this case is influenced by the trap inhomogeneity [11–17]. In addition, in the low-density regime a process of phase ordering kinetics [18–23] additionally modifies the scaling laws. Finally, we propose an experimental setup and parameters reachable by current technologies [24–26] which will enable us to observe the clear rate-independent hysteresis loop of nonzero width.

The system we focus on is an antiferromagnetic condensate of sodium atoms in a homogeneous magnetic field B, having positive magnetization such that $0 < M < N$. We restrict the model to one dimension, with the other degrees of freedom confined by a strong transverse potential with frequency $\omega_\perp$. The model Hamiltonian of the system is composed of two terms: the energy of the spin-1 system H_s and the energy shift H_{QZE} due to a homogeneous magnetic field. The first term is given by

$$H_s = \int dx \sum_{m_F} \psi^\dagger_{m_F} \left(-\frac{\hbar^2}{2\mu}\nabla^2 + \frac{1}{2}\mu\omega^2 x^2 \right) \psi_{m_F} + \int dx \left(\frac{c_0}{2} n^2 + \frac{c_2}{2} \mathbf{F}^2 \right), \tag{1}$$

where μ is the atomic mass, ω is a trap frequency, $n = \sum n_{m_F} = \sum \psi^\dagger_{m_F} \psi_{m_F}$ is the local atom density, and $\mathbf{F} = (\psi^\dagger f_x \psi, \psi^\dagger f_y \psi, \psi^\dagger f_z \psi)$ is the spin density, with $f_{x,y,z}$ the spin-1 matrices and $\psi^T = (\psi_1, \psi_0, \psi_{-1})$. The

 ©2018 American Physical Society

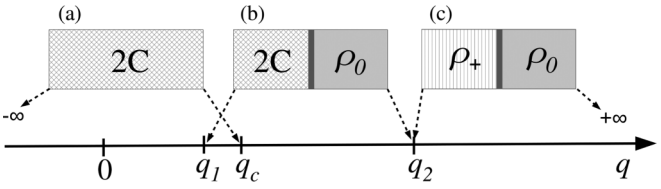

FIG. 1. Schematic structure of the mean-field ground state of the system versus q for positive magnetization $M > 0$. Dashed arrows indicate the stability regions of (a) the antiferromagnetic $2C$ state with atoms in the $m_F = \pm 1$ components, (b) the $2C + \rho_0$ state composed of two domains of the $2C$ and ρ_0 phases, the latter composed of atoms in the $m_F = 0$ component, and (c) the $\rho_+ + \rho_0$ state composed of two domains of ρ_0 and ρ_+, the latter composed of atoms in the $m_F = 1$ component [5]. The vertical thick lines in (b) and (c) illustrate domain walls.

spin-independent and spin-dependent interaction coefficients are $c_0 = 2\hbar\omega_\perp(2a_2 + a_0)/3$ and $c_2 = 2\hbar\omega_\perp(a_2 - a_0)/3$, where a_S is the s-wave scattering length for colliding atoms with total spin S. The coefficients c_0 and c_2 are both positive for sodium atoms. The linear Zeeman effect becomes irrelevant, since it is proportional to the conserved magnetization, while the quadratic Zeeman energy becomes essential,

$$H_{\mathrm{QZE}} = -qc_2\rho N_0, \tag{2}$$

where we dropped a constant term. Here N_0 is the number of atoms in the $m_F = 0$ Zeeman component, $\rho = N/L$ is the total density, L is the system size, and $q = AB^2/c_2\rho$ with $A = (g_I + g_J)^2\mu_B^2/16E_{\mathrm{HFS}}$, in which g_I and g_J are the gyromagnetic ratios of the electron and nucleus, μ_B is the Bohr magneton, and E_{HFS} is the hyperfine energy splitting. The value and sign of the quadratic Zeeman energy, through q, can be controlled using the magnetic field B or the microwave dressing [27].

We first concentrate on the case of a homogeneous system ($\omega = 0$). The ground-state structure of the uniform system can be found on the mean-field level by minimization of the mean-field energy functional in the subspace of fixed magnetization [5,6,28]. When the spin healing length $\xi_s = \hbar/\sqrt{2\mu c_2\rho}$ is much smaller than the system size L, the structure of the system ground state is composed of three states divided by two critical points at $q_1 = m^2/2$, where $m = M/N$ is the fractional magnetization, and $q_2 = 1/2$,[1] as illustrated in Fig. 1. The system is in the antiferromagnetic ground state when $q < q_1$ and in the phase separated state otherwise. Moreover, the analysis of the Bogoliubov spectrum [6] shows that the antiferromagnetic state is dynamically stable and it remains a local energy minimum up to the value $q_c = 1 - \sqrt{1 - m^2}$. It is easy to see that $q_1 \leqslant q_c$ for any m. A simultaneous stability of the two states may lead to the hysteresis phenomenon when dynamically changing q. We assume that the parameter q is

[1]The width of the domain wall is of the order of the spin healing length and the condition $\xi_s \ll L$ allows one to neglect the energy of the domain walls during derivation of q_1 and q_2 [5,6].

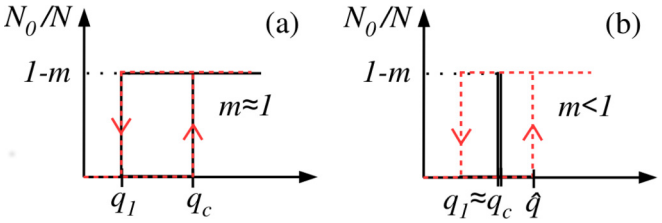

FIG. 2. Hysteresis in the system while crossing the critical points in the case of (a) a large and (b) a small width of the bistability region. The hysteresis loop in the small quench time limit is illustrated by dashed red lines and in the adiabatic limit by solid black lines.

tuned in the following way:

$$q(t) = \begin{cases} \alpha\frac{t}{\tau_Q}, & t \in (0,\tau_Q) \\ \alpha\left(2 - \frac{t}{\tau_Q}\right), & t \in (\tau_Q, t_{\max}), \end{cases} \tag{3}$$

where α sets the maximal value of q, τ_Q is the quench time, and $t_{\max}$ is the evolution time. The nucleation and growth of the ρ_0 phase can be characterized by the fraction of atoms in the $m_F = 0$ component. The relation of N_0/N versus q can take the form of the hysteresis loop of width $q_c - q_1$ set by the size of the bistability region. The width of the bistability region depends on the fractional magnetization m making the hysteresis phenomena qualitatively different in the two limits, $m \to 0$ and $m \to 1$, as illustrated in Fig. 2.

In the limit of macroscopic magnetization $m \to 1$, the region of bistability is large $q_c - q_1 \to 1/2$ and the hysteresis may become rate independent. The hysteresis area

$$S(\tau_Q) = \int_{q(\tau_Q)}^{q(t_{\max})} \frac{N_0(q)}{N} dq - \int_{q(0)}^{q(\tau_Q)} \frac{N_0(q)}{N} dq \tag{4}$$

is

$$S(\tau_Q) \approx (1 - m)(q_c - q_1) \tag{5}$$

while approximating the shape of the hysteresis loop by a rectangle of height $N_0/N \to 1 - m$ and width $q_c - q_1$, as represented in Fig. 2(a).

In the limit of small magnetization $m \to 0$ one can expect rate-dependent hysteresis as $q_c - q_1 \to 0$. The scaling of the hysteresis area (4) with the quench time τ_Q may exhibit a scaling law due to a nonadiabatic phase transition caused by finite quench times considered (3). In order to predict the corresponding scaling law we use the KZ theory [7–9] for the description of the nonadiabatic phase transition, which we have developed for the case of antiferromagnetic spinor condensates [29,30]. The KZ theory is a powerful tool which allows one to predict the scaling law for density of topological defects versus the quench rate based on the relation of characteristic timescales in terms of critical exponents, which are $z = 1$ and $\nu = 1/2$ for our system [6]. The theory is based on the adiabatic-impulse-adiabatic approximation, which implies that the scaling law is determined at the freeze-out time $\hat{t}$ when the dynamics of the system ceases to be adiabatic. The small parameter of the KZ theory is the distance from the critical point ε, which in the case of our system is $\varepsilon = q - q_c$. The KZ theory predicts $\varepsilon(\hat{t}) \propto \tau_Q^{1/(1+z\nu)}$ for the linear ramp we are considering. The scaling law of the hysteresis area (4)

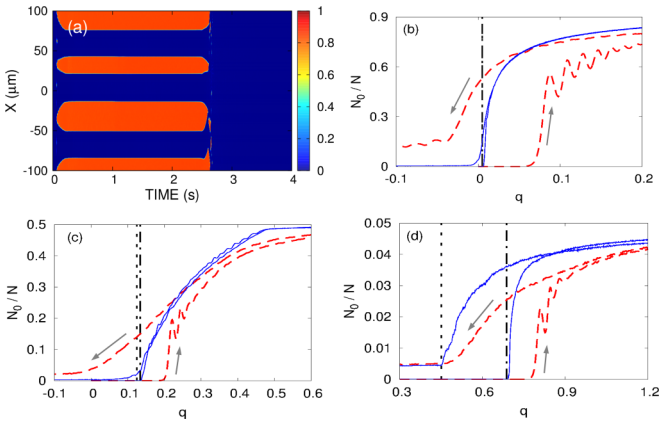

FIG. 3. (a) Evolution of density of the $m_F = 0$ component for $\tau_Q = 1.36$ s and $m = 0.5$. Also shown is the evolution of N_0/N as a function of q averaged over 50 realizations for a boxlike potential ($\omega = 0$) and (b) $m = 0.1$, (c) $m = 0.5$, and (d) $m = 0.95$. The thin red dashed line corresponds to $\tau_Q = 11$ ms and the blue solid one to $\tau_Q = 1.36$ s. The parameters q_1 and q_c are denoted by dotted and dot-dashed black lines, respectively. The gray arrows indicate the direction of evolution. The parameters are as follows: $N = 2\times10^7$, $\omega_\perp = 2\pi\times1000$ Hz, $L = 200$ μm, $\alpha = 3$, and $t_{\max} = 3\tau_Q$.

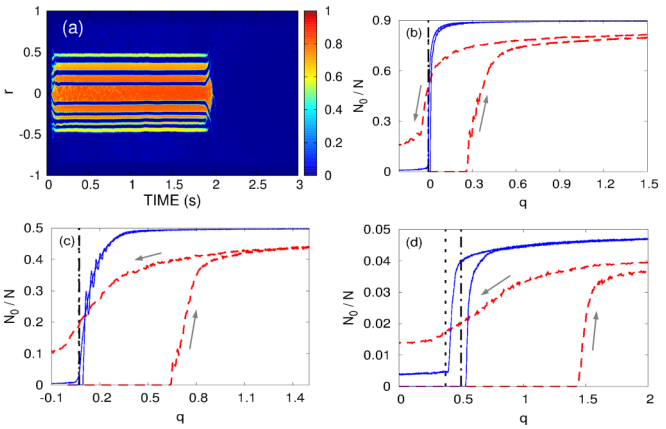

FIG. 4. (a) Evolution of density of the $m_F = 0$ component for $\tau_Q = 1$ s. Also shown is the evolution of N_0/N as a function of q averaged over 50 realizations for a harmonic trapping potential and (b) $m = 0.1$, (c) $m = 0.5$, and (d) $m = 0.95$. The thick red dashed line corresponds to $\tau_Q = 0.2$ s and the blue solid one to $\tau_Q = 8$ s. The parameters $q_1(0)$ and $q_c(0)$ are denoted by dotted and dot-dashed black lines, respectively. The gray arrows indicate the direction of evolution. The parameters are as follows: $N = 2\times10^6$, $\omega_\perp = 2\pi\times1000$ Hz, $\omega = 2\pi\times40$ Hz, $\alpha = 3$, and $t_{\max} = 3\tau_Q$.

is determined by the scaling of q at $\hat{t}$ or consistently by the distance from the critical point $\varepsilon(\hat{t}) = q(\hat{t}) - q_c$. By using our previous results for critical exponents [6], one can show that the scaling law for the hysteresis area (4) at $\hat{t}$ is

$$\hat{S}(\tau_Q) \propto q(\hat{t}) - q_c \propto \tau_Q^{-2/3}. \tag{6}$$

We test the above prediction in numerical simulations within the truncated Wigner approximation [31,32]. The dynamics of the system is then described by the set of time-dependent Gross-Pitaevskii equations

$$\begin{aligned} i\hbar\frac{\partial\psi_0}{\partial t} &= \left(-\frac{\hbar^2\nabla^2}{2\mu} + \frac{1}{2}\mu\omega^2x^2 + c_0n - q(t)c_2\rho\right)\psi_0 \\ &\quad + c_2[(n_1 + n_{-1})\psi_0 + 2\psi_0^*\psi_1\psi_{-1}], \\ i\hbar\frac{\partial\psi_{\pm1}}{\partial t} &= \left(-\frac{\hbar^2\nabla^2}{2\mu} + \frac{1}{2}\mu\omega^2x^2 + c_0n\right)\psi_{\pm1} \\ &\quad + c_2\left[(n_{\pm1} - n_{\mp1} + n_0)\psi_{\pm1} + \psi_{\mp1}^*\psi_0^2\right]. \end{aligned} \tag{7}$$

The initial state is the $2C$ state for $q = 0$ such that in momentum space $\psi_{m_F}(k,t=0) = \phi_{m_F} + \delta\phi_{m_F}$, with $|\phi_{m_F=\pm1}|^2 = (N \pm M)/2$, $|\phi_{m_F=0}|^2 = 0$, and stochastic noise $\langle\delta\phi^*_{m_F}(k)\delta\phi_{m'_F}(k')\rangle = \frac{1}{2}\delta_{m_F,m'_F}\delta_{k,k'}$, in amount of half a particle per momentum mode in all three m_F components is added.

In Fig. 3 we show examples of numerical simulation results for different fractional magnetizations in the large total atom limit $N = 2\times10^7$. Nucleation and growth of the ρ_0 phase and spin domains are clearly visible when the value of q exceeds the critical value [see density profiles in Fig. 3(a)]. Several domains are created, not just two as predicted for the ground state, due to nonideal adiabaticity of the quench. The number of domains decreases to 2 when increasing the quench rate τ_Q. Initial oscillations in N_0/N visible for shorter times in Figs. 3(b)–3(d) result from spin-mixing dynamics [33–35]. Indeed, for the smallest magnetization the hysteresis loop disappears as the quench time increases. On the other hand, the hysteresis loop of finite width is clearly visible and stable when the fractional magnetization tends to 1, demonstrating the rate-independent hysteresis.

We also study the system enclosed in an external harmonic trapping potential ($\omega \neq 0$). One can show, based on the Thomas-Fermi and local-density approximations, that the values of both q_1 and q_c are space dependent [11]. By introducing the Thomas-Fermi unit $r = x/x_{\rm TF}$, where $x_{\rm TF} = (3c_0N/2\mu\omega^2)^{1/3}$ is the Thomas-Fermi radius, the parameters q of interest are

$$q_1(r) = \frac{1}{2}\times\begin{cases}\frac{(1-r_1^2)^2}{1-r^2}, & |r|\in[0,r_1]\\ 1-r^2, & |r|\in[r_1,1]\end{cases} \tag{8}$$

and

$$q_c(r) = (1-r^2)[1-\sqrt{1-\tilde{m}(r)^2}], \tag{9}$$

where $r_1 = (1-m)^{1/3}$ and the density of local magnetization is $\tilde{m}(r) = (1-r_1^2)/(1-r^2)$ for $r\in[0,r_1]$ and $\tilde{m}(r) = 1$ otherwise. The inhomogeneity, arising as a result of the external trapping potential, introduces new physics. The width of the bistability region is not fixed but is space dependent. Moreover, particular parts of the system undergo a phase transition at different times, which additionally eliminates the bistability region. The growth of the ρ_0 phase not only depends on the reminiscence of the state history but is influenced much by the neighboring local phase due to tunneling of the local magnetization [11]. As a consequence, the width of the hysteresis loop is not strictly connected to the width of the bistability area. In Fig. 4 we show an example of the numerical simulation result for the evolution of density of the $m_F = 0$ component and N_0/N demonstrating the emergence of hysteresis.

In Fig. 5(a) we show scaling of the hysteresis area S versus ramp times τ_Q for the boxlike potential ($\omega = 0$). The two

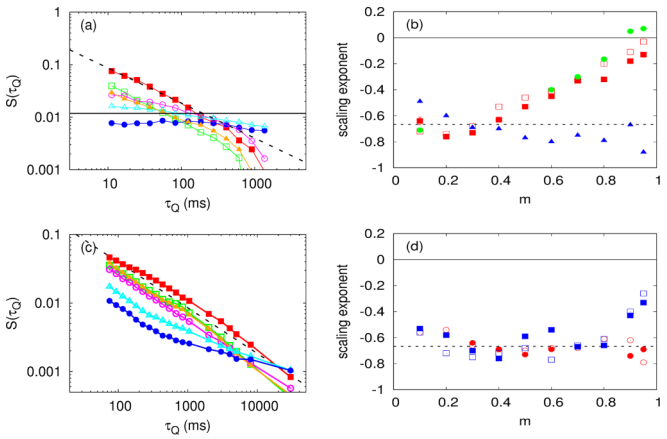

FIG. 5. Scaling of the hysteresis loop area $S(\tau_Q)$ with τ_Q for $m = 0.1$ (closed squares), $m = 0.3$ (open squares), $m = 0.5$ (closed triangles), $m = 0.7$ (open circles), $m = 0.9$ (open triangles), and $m = 0.95$ (closed circles) for the (a) box and (c) harmonic trap potentials. The dashed line shows $S(\tau_Q) \propto \tau_Q^{-2/3}$, while the solid line shows the value $(1-m)(q_c - q_1)$ for $m = 0.95$. (b) and (d) Scaling exponent of the hysteresis area versus fractional magnetization m obtained numerically by fitting a linear function to logarithms of numerical data presented in (a) and (c), respectively. The total numbers of atoms in (b) are $N = 2\times10^7$ (squares), $N = 6\times10^5$ (circles), and $N = 10^4$ (triangles). The total number of atoms in (d) is $N = 2\times10^6$ and the circles (squares) mark the scaling exponent of the hysteresis area for $\tau_Q < 1$ s ($\tau_Q > 1$ s). In (b) and (d) open symbols correspond to $\alpha = 1.5$ and closed ones to $\alpha = 3$. Notice that error bars are shown for (b) $N = 2\times10^7$ and (d) $N = 2\times10^6$, but they are of the order of the symbol size.

limiting cases $m \to 0$ and $m \to 1$ are clearly visible. Interestingly, even for intermediate fractional magnetizations, the hysteresis area S is subject to the scaling law but with a different exponent. We gather the resulting scaling exponents versus fractional magnetization in Fig. 3(b). While the results for the largest and moderate atom numbers follow our predictions, the results for the smallest atom number ($N = 10^4$ marked by triangles) are different. This is because the widths of domain walls increase when N decreases and the energy of the domain wall cannot be neglected in the derivation of q_1. In other words, the effect of the finite size of the system increases the value of q_1 up to q_c (see Fig. 1). Consequently, the width of the bistability region tends to 0 and the hysteresis phenomenon becomes rate dependent even for large fractional magnetizations, as demonstrated in Fig. 5(b). The resulting scaling exponent in the low-density regime follows the KZ theory [6] slightly modified by the phase ordering kinetics process [18].

The case of a trapped system ($\omega \neq 0$) is qualitatively different because the scaling of the hysteresis loop area exhibits a double law for macroscopic magnetizations $m \to 1$, as illustrated in Fig. 5(c) for $N = 2\times10^6$. The KZ theory for the trapped case in the local-density approximation [11] gives $\hat{S} \propto \tau_Q^{-2/3}$, which is confirmed by numerical calculations presented in Fig. 5(d) for small τ_Q only. The numerical results deviate from the KZ theory predictions for macroscopic magnetizations in the adiabatic quench times limit.

While performing the experiment with the largest number of atoms ($N = 2\times10^7$) appears to be unrealistic, in part because of strong two- and three-body losses, we find a regime of parameters in which the hysteresis and scaling laws may be observed, as shown by green dots in Fig. 5(b). We propose the use of a moderate number of atoms $N = 6\times10^5$ and a tight transverse confinement of $\omega_\perp = 2\pi\times2800$ Hz, which allows one to avoid transverse excitations. The latter tight confinement requirement may be reduced to $\omega_\perp = 2\pi\times100$ Hz in the nonpolynomial Gross-Pitaevskii regime [36], as long as the ratio $c_2 n/\hbar\omega_\perp$ is small, which ensures the absence of transverse *spin* excitations. The spatial extent of the condensate in the longitudinal direction must be large enough so that sufficiently many domains are observed ($L > 600$ μm), which appears to be within the reach of state-of-the-art experiments [37]. With these parameters and typical linear densities of 10^{14} atoms/cm^3, the lifetime of the condensate due to one-, two-, and three-body losses may be estimated at around 20 s [38], which should allow for the observation of rate-independent hysteresis predicted here.

In summary, an antiferromagnetic spinor condensate exhibits hysteresis controlled by the magnetic field, which may be practical in its further applications. We investigated hysteresis during the phase transition, showing that it is rate independent for a homogeneous system in the limit of large magnetizations only. In all other cases, the hysteresis is rate dependent and the area of its loop is subject to the universal scaling law, which we explained based on the KZ theory.

We acknowledge support from the National Science Center Grants No. DEC-2015/18/E/ST2/00760, No. DEC-2015/17/B/ST3/02273, and No. DEC-2015/17/D/ST2/03527.

[1] S. Eckel, J. G. Lee, F. Jendrzejewski, N. Murray, C. W. Clark, C. J. Lobb, W. D. Phillips, M. Edwards, and G. K. Campbell, Nature (London) **506**, 200 (2014).
[2] A. Roussou, G. D. Tsibidis, J. Smyrnakis, M. Magiropoulos, N. K. Efremidis, A. D. Jackson, and G. M. Kavoulakis, Phys. Rev. A **91**, 023613 (2015).
[3] M. J. Davis and K. Helmerson, Nature (London) **506**, 166 (2014).
[4] A. Trenkwalder, G. Spagnolli, G. Semeghini, S. Coop, M. Landini, P. Castilho, L. Pezzè, G. Modugno, M. Inguscio, A. Smerzi, and M. Fattori, Nat. Phys. **12**, 826 (2016).
[5] M. Matuszewski, T. J. Alexander, and Y. S. Kivshar, Phys. Rev. A **80**, 023602 (2009).
[6] E. Witkowska, J. Dziarmaga, T. Świsłocki, and M. Matuszewski, Phys. Rev. B **88**, 054508 (2013).
[7] W. H. Żurek, Nature (London) **317**, 505 (1985).
[8] W. H. Żurek, Acta Phys. Pol. B **24**, 1301 (1993).
[9] W. H. Żurek, Phys. Rep. **276**, 177 (1996).
[10] W. Casteels, F. Storme, A. Le Boité, and C. Ciuti, Phys. Rev. A **93**, 033824 (2016).
[11] T. Świsłocki, E. Witkowska, and M. Matuszewski, Phys. Rev. A **94**, 043635 (2016).

[12] W. H. Żurek, Phys. Rev. Lett. **102**, 105702 (2009).
[13] J. Dziarmaga and M. M. Rams, New J. Phys. **12**, 055007 (2010).
[14] J. Sabbatini, W. H. Żurek, and M. J. Davis, New J. Phys. **14**, 095030 (2012).
[15] A. del Campo, T. W. B. Kibble, and W. H. Żurek, J. Phys.: Condens. Matter **25**, 404210 (2013).
[16] H. Saito, Y. Kawaguchi, and M. Ueda, J. Phys.: Condens. Matter **25**, 404212 (2013).
[17] A. del Campo and W. H. Zurek, Int. J. Mod. Phys. A **29**, 1430018 (2014).
[18] A. J. Bray, Adv. Phys. **43**, 357 (1994).
[19] L. M. Symes and P. B. Blakie, Phys. Rev. A **96**, 013602 (2017).
[20] S. Mukerjee, C. Xu, and J. E. Moore, Phys. Rev. B **76**, 104519 (2007).
[21] K. Kudo and Y. Kawaguchi, Phys. Rev. A **88**, 013630 (2013).
[22] K. Kudo and Y. Kawaguchi, Phys. Rev. A **91**, 053609 (2015).
[23] L. A. Williamson and P. B. Blakie, Phys. Rev. Lett. **116**, 025301 (2016).
[24] D. Jacob, L. Shao, V. Corre, T. Zibold, L. De Sarlo, E. Mimoun, J. Dalibard, and F. Gerbier, Phys. Rev. A **86**, 061601(R) (2012).
[25] C. Frapolli, T. Zibold, A. Invernizzi, K. Jiménez-García, J. Dalibard, and F. Gerbier, Phys. Rev. Lett. **119**, 050404 (2017).
[26] S. Kang, S. W. Seo, J. H. Kim, and Y. Shin, Phys. Rev. A **95**, 053638 (2017).
[27] F. Gerbier, A. Widera, S. Fölling, O. Mandel, and I. Bloch, Phys. Rev. A **73**, 041602 (2006).
[28] W. Zhang, S. Yi, and L. You, New J. Phys. **5**, 77 (2003).
[29] T. Świsłocki, E. Witkowska, J. Dziarmaga, and M. Matuszewski, Phys. Rev. Lett. **110**, 045303 (2013).
[30] E. Witkowska, T. Świsłocki, and M. Matuszewski, Phys. Rev. A **90**, 033604 (2014).
[31] M. J. Steel, M. K. Olsen, L. I. Plimak, P. D. Drummond, S. M. Tan, M. J. Collett, D. F. Walls, and R. Graham, Phys. Rev. A **58**, 4824 (1998).
[32] A. Sinatra, C. Lobo, and Y. Castin, Phys. Rev. Lett. **87**, 210404 (2001).
[33] H. Pu, C. K. Law, S. Raghavan, J. H. Eberly, and N. P. Bigelow, Phys. Rev. A **60**, 1463 (1999).
[34] W. Zhang, D. L. Zhou, M.-S. Chang, M. S. Chapman, and L. You, Phys. Rev. A **72**, 013602 (2005).
[35] M.-S. Chang, Q. Qin, W. Zhang, L. You, and M. S. Chapman, Nat. Phys. **1**, 111 (2005).
[36] L. Salasnich, A. Parola, and L. Reatto, Phys. Rev. A **65**, 043614 (2002).
[37] W. von Klitzing (unpublished).
[38] A. Görlitz, T. L. Gustavson, A. E. Leanhardt, R. Löw, A. P. Chikkatur, S. Gupta, S. Inouye, D. E. Pritchard, and W. Ketterle, Phys. Rev. Lett. **90**, 090401 (2003).